Available online at www.sciencedirect.com
ScienceDirect
Catalysis Today 116 (2006) 485–497
CATALYSIS TODAY
www.elsevier.com/locate/cattod

SBA-15 supports modified by Ti and Zr grafting for NiMo hydrodesulfurization catalysts

Oliver Y. Gutiérrez [a], Gustavo A. Fuentes [b], Cecilia Salcedo [a], Tatiana Klimova [a,*]

[a] *Facultad de Química, Universidad Nacional Autónoma de México (UNAM), Cd. Universitaria, Coyoacán, 04510, México D.F., Mexico*
[b] *Área de Ingeniería Química, Universidad Autónoma Metropolitana-Iztapalapa (UAM-I), Av. Michoacán y Purísima, Iztapalapa, 09340, México D.F., Mexico*

Available online 1 August 2006

Abstract

A series of Ti- and Zr-containing mesoporous SBA-15 supports and their respective NiMo catalysts were prepared to study the effect of the Ti and Zr loading into the support on the characteristics of Ni and Mo surface species and their catalytic activity in the 4,6-dimethyldibenzothiophene hydrodesulfurization (HDS). Ti and Zr-containing SBA-15 solids with different metal loading (up to 19 wt.% of TiO_2 or 22 wt.% of ZrO_2) were prepared by chemical grafting. The solids prepared were characterized by N_2 physisorption, X-ray diffraction (XRD), UV–vis diffuse reflectance spectroscopy (DRS), temperature-programmed reduction (TPR), chemical analysis and HRTEM. The results show that Ti- and Zr-SBA-15 supports with highly dispersed Ti and Zr species can be obtained without substantial loss of SBA-15 characteristics. Zr grafted species showed somewhat better dispersion on the SBA-15 surface than the corresponding Ti counterparts. It was found that TiO_2 and, especially, ZrO_2 incorporation in the SBA-15 support leads to stronger interaction of Mo and Ni species with the support providing better dispersion to the oxidic and sulfided metal species (XRD, TPR, HRTEM). NiMo catalysts supported on Ti- and Zr-containing SBA-15 showed high activity in 4,6-dimethyldibenzothiophene HDS. It can be concluded therefore that SBA-15 materials grafted with Ti or Zr species show promising features as supports for Mo-based hydrotreating catalysts.

Keywords: SBA-15; Mesoporous molecular sieves; Titania; Zirconia; Chemical grafting; NiMo catalysts; Hydrodesulfurization; 4,6-Dimethyldibenzothiophene

1. Introduction

Nowadays, the current demand of high quality low sulfur transportation fuels (gasoline, diesel) is growing because of the necessity of solving environmental problems induced by SO_x emissions. For this purpose, more active hydrodesulfurization (HDS) catalysts are requested from industry. Traditionally, alumina-supported Mo catalysts promoted by Co and/or Ni have been used for hydrotreatment of oil feedstock (HDT) [1,2]. It is well known that the catalytic performance of HDS catalysts depends not only on the nature and structure of the active phase but also on the chemical and textural characteristics of the support used, since the change of the support affects the surface properties of the catalyst. Recently, in order to obtain more active HDS catalysts, many approaches have been followed, among which variation of support is an important one. Different materials have been assayed as new supports for HDS catalysts, namely, silica [3,4], zirconia [5–7], titania [3,7,8], carbon [9], mixed oxides (ZrO_2–Al_2O_3 [10–12], ZrO_2–SiO_2 [12,13], ZrO_2–TiO_2 [14]), mesoporous materials like MCM-41 [15–19], SBA-15 [19,20], etc. A detailed analysis of the support effect can be found in recent reviews [21,22].

Among different supports and their combinations, TiO_2 and ZrO_2 have attracted attention due to the higher intrinsic HDS activity demonstrated by Mo catalysts supported on these oxides in comparison with alumina-supported counterpart [5,8,11,23]. In addition, it was found that NiMo catalyst supported on ZrO_2 has higher catalytic activity in thiophene HDS than that supported on TiO_2 [7]. However, pure titania and zirconia supports present one important disadvantage: they generally have low surface area and porosity, and despite the high intrinsic activity (per Mo atom), the specific activity (per gram of catalyst) remained lower than on alumina [5,24]. Because of this problem, some attempts to obtain titania- or

* Corresponding author. Tel.: +52 55 56225371; fax: +52 55 56225371.
E-mail address: klimova@servidor.unam.mx (T. Klimova).

0920-5861/$ – see front matter © 2006 Elsevier B.V. All rights reserved.
doi:10.1016/j.cattod.2006.06.035

zirconia-based supports with high surface area have been made in recent years through the use of alternative preparation methods. Thus, Chiyoda Corporation successfully developed a novel mesoporous TiO_2 with a specific surface area of 120 m^2/g that provides the opportunity of preparing the catalyst with a good Mo dispersion up to 10–12 wt.% Mo loading [25]. In line with this, amorphous and tetragonal zirconia supports with high specific surface area (192–278 m^2/g) were also synthesized and used for preparation of highly loaded NiMo catalysts. Prepared catalysts resulted to be more active in thiophene HDS and hydrogenation of tetraline than alumina-supported analogs [5]. Another possibility to achieve TiO_2 or ZrO_2 supports of high surface area is to combine a support with appropriate textural properties with titanium or zirconium oxides. Thus, promising results were obtained when titania was incorporated on the surface of mesoporous molecular sieve MCM-41 [26]. A substantially better dispersion of Mo was observed on MCM-41 supports modified with TiO_2 by post-synthetic methods. In another work [27], a Zr-HMS material was used to prepare Mo HDS catalysts, which showed higher catalytic activity than the reference Mo/SiO_2 material in thiophene HDS. It was found that zirconium improves hydrogenation activities of the samples. However, the MCM-41 and HMS type materials have poor stability [28,29] and relatively small pores (about 20–35 Å diameter), which can be easily blocked by HDS active phases [27]. These disadvantages represent a serious limitation to the practical applications of MCM-41 or HMS-based formulations.

Recently, a novel family of mesoporous silicas (SBA) was synthesized by using neutral organic triblock copolymers [30–32]. These new materials have larger pores, thicker pore walls and higher hydrothermal stability compared to MCM-41. Purely siliceous SBA-15 material has already been tested as a support for WS_2 active phase. However, because of very weak metal-support interaction, ultrasonic deposition of WS_2 had been used to achieve a better dispersion of W sulfided species [20]. In our group, a series of Al- and Ti-containing mesoporous molecular sieves SBA-16 with cubic structure ($Im\bar{3}m$) and the respective NiMo catalysts were prepared and tested in 4,6-dimethyldibenzothiophene HDS [33,34]. It was found that aluminum or titanium incorporation in the SBA-16 support provides better dispersion to deposited Ni and Mo active species and increases their catalytic activity in HDS of 4,6-dimethyldibenzothiophene, one of the most refractory sulfur compounds. Different methods for the preparation of SBA-type supports modified with heteroatoms (Al, Ti) were tested, namely, addition of Al or Ti species during hydrothermal synthesis of SBA-16 support (synthetic method), and two post-synthetic methods (chemical grafting and incipient wetness impregnation), where heteroatom species are deposited on the surface of already formed and calcined SBA material. Post-synthetic methods resulted to be more suitable for the preparation of SBA solids containing heteroatoms.

In the present work, with the aim of obtaining novel SBA-type supports that provide good Mo dispersion and therefore high HDS activity, we prepared and characterized a series of Ti- and Zr-modified SBA-15 molecular sieves and their respective NiMo catalysts, which were evaluated in the 4,6-dimethyldibenzothiophene (4,6-DMDBT) HDS reaction. Purely siliceous SBA-15, which possesses a well-ordered two-dimensional (2D) hexagonal ($p6mm$) array of mesopores, was selected as a parent material to be modified with titania or zirconia. SBA-15 materials prepared with triblock poly(ethylene oxide)–poly(-propylene oxide)–poly(ethylene oxide) copolymers ($EO_mPO_nEO_m$) exhibit large surface areas (690–920 m^2/g) and pore volumes (0.80–1.23 mL/g), pore sizes between 47 and 89 Å, and unusually thick walls (31–53 Å) providing them remarkable hydrothermal stability [30–32,35]. In addition, these materials have the unique dual pore system formed by hexagonally arranged cylindrical mesopores with micropores within the walls, which provide connectivity between large pores [35].

Titania and zirconia were incorporated in this parent SBA-15 by chemical grafting [26,36]. This method was chosen because of the advantages it has in comparison with the incorporation of heteroatoms into the SBA structure during hydrothermal synthesis of SBA materials or incipient wetness impregnation. Thus, (i) chemical grafting allows deposition of highly dispersed species on the surface of the parent SBA without altering its structure and texture, (ii) grafted species are located on the support surface, this makes them all accessible for the interaction with NiMo active species [26,34,36]. In resume, chemical grafting technique permits modification of the chemical properties of solid surface without substantial changes in the physical characteristics of the material.

The aim of the present work is to study the effect that incorporation of different amounts of titania or zirconia on the surface of SBA-15 by chemical grafting has on the characteristics of the Ni- and Mo-supported species and the performance of the obtained catalysts in the 4,6-dimethyldibenzothiophene hydrodesulfurization.

2. Experimental

2.1. Support and catalyst preparation

The pure siliceous SBA-15 material used in this paper has been synthesized according to the procedure described elsewhere [30,31]. Ti- and Zr-modified SBA-15 supports were prepared by chemical grafting [26,34]. Titanium(IV) isopropoxide (Ti(*i*-PrO)$_4$, 97%, Aldrich) and zirconium(IV) propoxide (Zr(*n*-PrO)$_4$, 70 wt.% solution in 1-propanol, Aldrich) were used as titania and zirconia sources, respectively, and dry ethanol as the solvent (EtOH, Aldrich, 99.999%). In the grafting procedure, calcined SBA-15 was slurried in dry EtOH containing Ti(*i*-PrO)$_4$ or Zr(*n*-PrO)$_4$ for 8 h at room temperature. To eliminate excess of Ti(*i*-PrO)$_4$ or Zr(*n*-PrO)$_4$, the filtered material was washed with dry EtOH three times. The solid was then dried in air at room temperature and calcined in static air at 550 °C for 5 h. Hereafter, Ti- or Zr-containing SBA-15 materials will be denoted as M-SBA-15(x) samples, where M represents the metal (M = Ti or Zr) and x shows wt.% of MO_2 in the sample.

NiMo/SBA-15 catalysts were prepared by a standard incipient wetness technique. The calcined supports were

impregnated successively using aqueous solutions of ammonium heptamolybdate, $(NH_4)_6Mo_7O_{24}{\cdot}4H_2O$ (Aldrich), and nickel nitrate, $Ni(NO_3)_2{\cdot}6H_2O$ (Aldrich). Mo was impregnated first. After each impregnation, the catalysts were dried (100 °C, 24 h) and calcined (500 °C, 4 h). In addition, NiMo catalyst supported on γ-alumina was prepared for comparison purposes. The nominal composition of the catalysts was 12 wt.% of MoO_3 and 3 wt.% of NiO. Hereafter, the catalysts will be denoted as NiMo/corresponding support.

2.2. Support and catalyst characterization

The supports and catalysts were characterized by N_2 physisorption, X-ray diffraction (XRD), UV–vis diffuse reflectance spectroscopy (DRS), temperature-programmed reduction (TPR), SEM-EDX and HRTEM. N_2 adsorption/desorption isotherms were measured with a Micromeritics ASAP 2000 automatic analyzer at liquid N_2 temperature. Prior to the experiments, the samples were degassed ($p < 10^{-1}$ Pa) at 270 °C for 6 h. Specific surface areas were calculated by the BET method (S_{BET}), the total pore volume (V_p) was determined by nitrogen adsorption at a relative pressure of 0.98 and pore size distributions from the desorption isotherms by the BJH method. The mesopore diameter (D_P) corresponds to the maximum of the pore size distribution. The micropore area (S_μ) was estimated using the correlation of *t*-Harkins & Jura (*t*-plot method). XRD patterns were recorded in the $3^\circ \leq 2\Theta \leq 90^\circ$ range on a Siemens D5000 diffractometer, using Cu Kα radiation (λ = 1.5406 Å) and a goniometer speed of 1° (2Θ) min^{-1}. Small-angle XRD (2Θ = 1–10°) was performed on a Bruker D8 Advance diffractometer using small divergence and scattering slits of 0.05°. The a_0 unit-cell parameter was estimated from the position of the (1 0 0) diffraction line ($a_0 = d_{100} \times 2/\sqrt{3}$) [12]. Pore wall thickness, δ, was assessed by subtracting D_P from the a_0 unit-cell parameter which corresponds to the distance between the centers of adjacent mesopores. UV–vis–NIR electronic spectra of the samples were recorded in the wavelength range 250–2500 nm using a Cary |5E| spectrophotometer equipped with a diffuse reflectance attachment. $BaSO_4$ was used as reference. TPR experiments were carried out in an automated ISRI-RIG-100 characterization system equipped with a TC detector. In the TPR experiments, the samples were pretreated *in situ* at 500 °C for 2 h under air flow and cooled in an Ar stream. The reduction step was performed with an Ar/H_2 mixture, with a heating rate of 10 °C/min, up to 1000 °C. The chemical analysis of the Ti- and Zr-containing SBA-15 supports was made by Desert Analytics (USA). High resolution transmission electron microscopy (HRTEM) studies were performed using a Jeol 2010 microscope (resolving power 1.9 Å). The solids were ultrasonically dispersed in heptane and the suspension was collected on carbon coated grids. Slab length and layer stacking distributions of MoS_2 crystallites in each sample were established from the measurement of at least 300 crystallites detected on several HRTEM pictures taken from different parts of the same sample dispersed on the microscope grid.

2.3. Catalytic activity

The 4,6-DMDBT HDS activity tests were performed in a batch reactor at 300 °C and 7.3 MPa total pressure for 8 h. Prior to the catalytic activity evaluation, the catalysts were sulfided *ex situ* in a tubular reactor at 400 °C for 4 h in a stream of 15 vol.% of H_2S in H_2 under atmospheric pressure. The sulfided catalysts (0.15 g) were transferred in an inert atmosphere (Ar) to a batch reactor (Parr) containing 40 mL of 4,6-DMDBT solution in *n*-hexadecane (0.024 mol/L). The course of the reaction was followed by withdrawing aliquots each hour and analyzing them on an HP-6890 chromatograph. To corroborate product identification, the product mixture was analyzed on a Hewlett Packard GC–MS instrument.

3. Results and discussion

3.1. Supports

Fig. 1 presents TEM micrographs of the parent SBA-15 solid prepared by reaction at 35 °C for 20 h with following hydrothermal treatment at 80 °C for 48 h. It was observed that the solid is formed by grains of relatively uniform size (typically 200–300 nm diameter and 700–1000 nm long). A well-ordered hexagonal array of mesopores is observed for this sample when the electron beam is parallel to the main axis of the cylindrical pores. When electron beam is perpendicular to the main axis, the cylindrical pores are viewed from the side as a stripped image. The distance between the centers of two adjacent pores is about 100 Å, and the pore diameter is about 60 Å.

The small-angle XRD pattern of the same calcined SBA-15 material exhibits three well-resolved peaks characteristic of SBA-15 [30,31], namely, a very intense peak at about 1.0° (2Θ) and two distinct weak peaks between 1.5° and 2.0° (2Θ) (Fig. 2). These XRD signals are indexable as (1 0 0), (1 1 0) and (2 0 0) reflections associated with *p6mm* hexagonal symmetry. The high-intensity (1 0 0) peak reflects a *d*-spacing of 88.3 Å and the following peaks have *d* values (51.6 Å for (1 1 0) peak and 45.0 Å for (2 0 0) peak) consistent with a bi-dimensional hexagonal arrangement of the pores with a unit-cell parameter a_0 = 102 Å.

The SBA-15 material shows surface area of 840 m^2/g, micropore area of 131 m^2/g and total pore volume of 1.117 cm^3/g (Table 1). Fig. 3 shows the nitrogen adsorption–desorption isotherm of this material. The isotherm is of type IV with a H1 hysteresis loop. The shape of the N_2 adsorption–desorption isotherm is characteristic for a well-formed SBA-15 material. The uniform mesopore diameter of SBA-15 sample is equal to 56 Å. Taking into account the distance between pore centers (a_0) measured by small-angle XRD, the pore wall thickness (δ) for this sample can be estimated to be equal to 46 Å. The results from XRD and N_2 physisorption calculations are well in line with the corresponding values measured directly from TEM images.

Two Ti-containing SBA-15 samples and two Zr-containing ones were prepared by chemical grafting technique. The

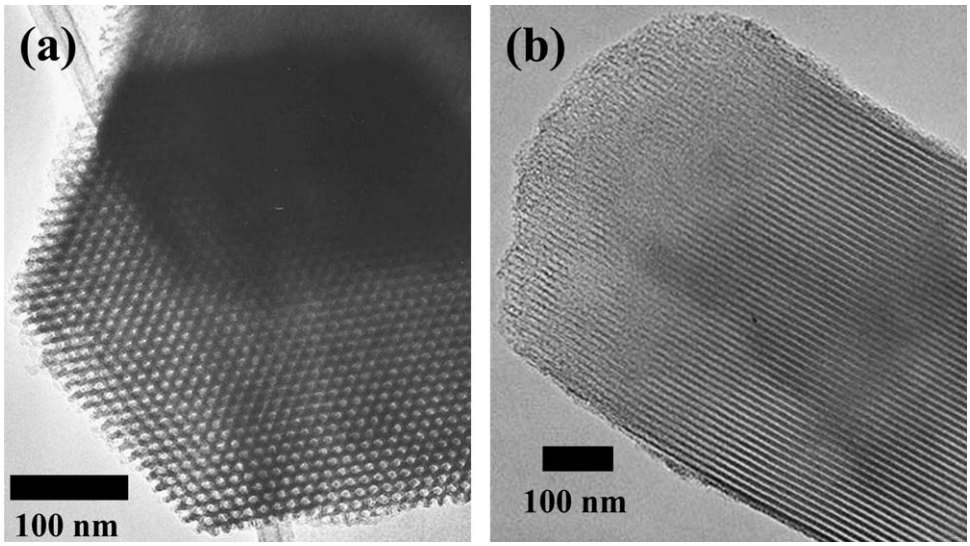

Fig. 1. Transmission electron microscopy images of the SBA-15 support. Electron beam parallel (a) and perpendicular (b) to the main axis of the pores.

concentration of metal alkoxide solution used in grafting procedure was changed in order to reach different metal loadings in Ti- and Zr-grafted SBA-15 solids. The expected theoretical metal oxide loadings would be 11 and 25 wt.% of TiO_2 for Ti-SBA-15 samples, and 17 and 40 wt.% of ZrO_2 for Zr-SBA-15 supports. The real TiO_2 or ZrO_2 loadings in the synthesized materials are given in Table 1. The results from chemical analysis show that Ti-SBA-15(11) and Zr-SBA-15(17) have the chemical composition similar to the expected one. This result shows that in this case almost all Ti or Zr species from solution reacted with SBA-15 surface. However, when the concentration of Ti or Zr species in the solution was increased, it was not possible to graft all of them on the SBA-15 material. The saturation of the SBA-15 surface with Ti or Zr species was reached at about 19.2 wt.% of TiO_2 or 22.4 wt.% of ZrO_2. This result can be rationalized taking into account that the immobilization of Ti or Zr species on SBA-15 surface by grafting is a result of the chemical interaction of corresponding alkoxides with silanol groups of the support, whereas the Ti or Zr in excess was eliminated by washing with dry ethanol. On the basis of this result, the monolayer capacity of SBA-15 surface can be estimated as about 2.35 Ti atoms/nm^2 or 2.02 Zr atoms/nm^2. These values are slightly below the silanol surface density of ~3.7 OH/nm^2 that has been reported previously for SBA-15 material [37]. From the above results, it can be inferred, therefore, that the monolayer-like distribution of metal species was reached in both cases (Ti and Zr), in which each titanium or zirconium atom is retained on the surface by one or two M–O–Si linkages. In addition, the existence of some isolated hydroxyls inert to the interaction with titanium or zirconium alkoxides at room temperature, can also be expected on the surface of the parent SBA-15 material, as it has been previously observed for different silica supports [38].

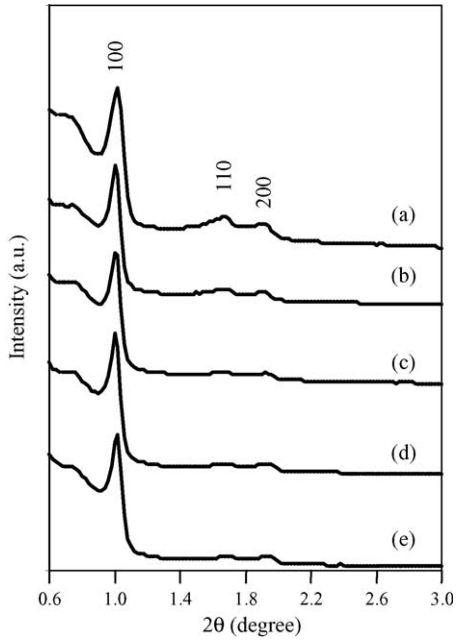

Fig. 2. Small-angle XRD patterns of SBA-15 (a); Ti-SBA-15(11) (b); Ti-SBA-15(19) (c); Zr-SBA-15(17) (d); Zr-SBA-15(22) (e) supports.

The textural and structural characteristics (surface area S_{BET}, micropore area S_μ, total pore volume V_P, micropore volume V_μ, pore diameter D_P, unit-cell parameter a_0 and pore wall thickness δ) of Ti- and Zr-containing SBA-15 supports are given in Table 1. It can be observed that titania and zirconia grafting on the SBA-15 surface results in a decrease of area and pore volume values. Thus, BET surface area decreases to 690–543 m^2/g and micropore area to 114–102 m^2/g after Ti and Zr incorporation. This decrease is larger for Zr-containing supports that can be due, probably, to higher MO_2 weight loading in this case. Total pore volume and micropore volume follow similar tendency after Ti and Zr incorporation into SBA-15 support. It should be mentioned, however, that pore diameter, unit-cell parameter and pore wall thickness did not suffer a significant change after Ti or Zr incorporation. Small-angle XRD patterns of Ti- and Zr-SBA-15 samples (Fig. 2b–e)

Table 1
Textural characteristics and chemical compositions of SBA-15 molecular sieves

Catalyst	MO_2 (wt.%)[a]	M (atoms/nm^2)	S_{BET} (m^2/g)	S_μ (m^2/g)	V_P (cm^3/g)	V_μ (cm^3/g)	D_P (Å)	a_0 (Å)	δ (Å)
SBA-15	–	–	840	131	1.117	0.051	56	102	46
Ti-SBA-15(11)	11.1	1.21	690	114	0.938	0.045	55	102	47
Ti-SBA-15(19)	19.2	2.35	614	112	0.785	0.045	57	102	45
Zr-SBA-15(17)	16.8	1.36	605	102	0.813	0.041	57	102	45
Zr-SBA-15(22)	22.4	2.02	543	102	0.706	0.041	57	102	45

[a] Determined by chemical analysis (M = Ti, Zr).

are similar to that of pure-siliceous parent SBA-15. It can be clearly observed, that the position of the reflections characteristic for SBA-15 material and their intensities did not change after Ti or Zr grafting indicating that the long-range periodicity order of the SBA-15 sample was preserved intact. Nitrogen adsorption–desorption isotherms of the Ti- and Zr-containing SBA-15 samples are shown in Fig. 3. Titanium and zirconium incorporation in the SBA-15 by grafting technique does not produce changes in the characteristic shape of the isotherm, with the exception of some decrease in the amount of adsorbed N_2 (Fig. 3), indicating that incorporation of both metals (Ti and Zr) does not affect the original pore structure of the parent SBA-15 material. All the above results point out high dispersion of grafted Ti and Zr species.

Additional information about TiO_2 and ZrO_2 dispersion in the series of Ti- and Zr-SBA-15 materials was obtained by UV–vis diffuse reflectance spectroscopy (Fig. 4). According to literature data, the DRS spectrum of bulk TiO_2-anatase exhibits a broad absorption at ~330 nm with an absorption edge at about 390 nm due to ligand-to-metal charge transfer (LMCT) between the O^{2-} ligand and the titanium(IV) ion [36]. No absorptions arise from silica, which is transparent in this region of the UV–vis spectrum (Fig. 4A(a)). In the DRS spectra of Ti-SBA-15(11) and (19) samples, the absorption band maximum is observed at 225 nm (Fig. 4A(b) and (c)). The band at *ca.* 230 nm has been observed for various titanosilicate zeolite materials and has been assigned to LMCT transitions involving isolated Ti atoms in tetrahedral (T_d) coordination [36,39]. The shoulder at *ca.* 270 nm observed in the DRS spectra of Ti-SBA-15 samples, indicates the presence of some isolated or partially polymerized octahedral (O_h) titanium species (Ti–O–Ti clusters) [36,39,40]. The detailed analysis of the spectra (b) and (c) in Fig. 4A shows that an increase in Ti loading in the samples produces not only an increase in the intensity of the UV–vis DRS spectra, but also changes the ratio between tetrahedral and octahedral Ti species, increasing the proportion of the latter. The absence of an absorption at ~330 nm indicates that the samples prepared by the grafting method are free from anatase phase. This result is well in line with observations made by powder XRD and Raman spectroscopy, where the formation of any kind of TiO_2 or ZrO_2 crystalline phases was not detected. The band-gap values of TiO_2-containing SBA-15 samples were evaluated from their DRS data by plotting the square of the

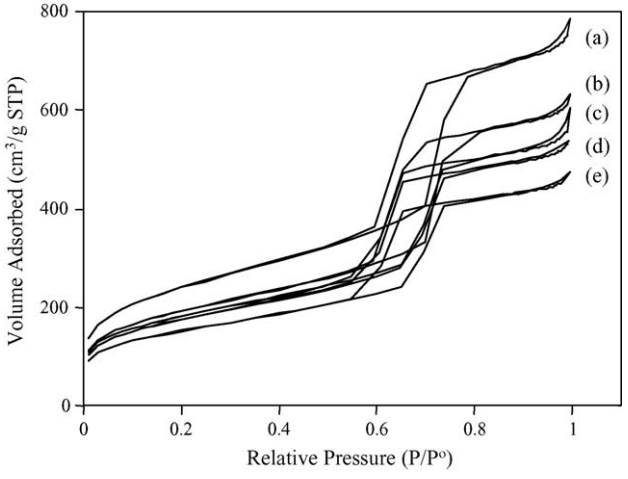

Fig. 3. Nitrogen adsorption–desorption isotherms of SBA-15 type supports: SBA-15 (a); Ti-SBA-15(11) (b); Ti-SBA-15(19) (c); Zr-SBA-15(17) (d); Zr-SBA-15(22) (e).

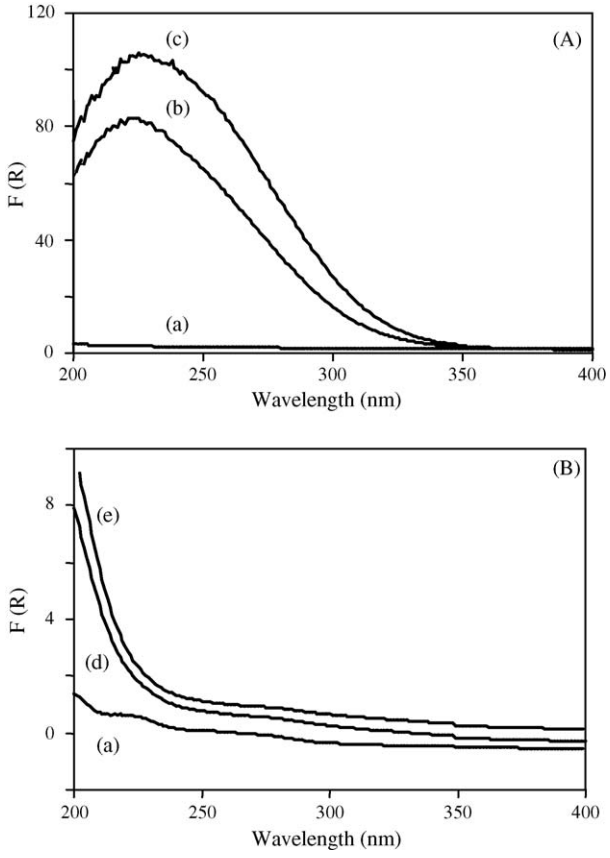

Fig. 4. UV–vis spectra of SBA-15 (a); Ti-SBA-15(11) (b); Ti-SBA-15(19) (c); Zr-SBA-15(17) (d); Zr-SBA-15(22) (e) supports.

Table 2
Textural characteristics of NiMo catalysts supported on SBA-15 supports

Catalyst	S_{BET} (m^2/g)	S_μ (m^2/g)	V_P (cm^3/g)	V_μ (cm^3/g)	D_P (Å)	a_0 (Å)	δ (Å)
NiMo/SBA-15	550	71	0.784	0.026	55	102	47
NiMo/Ti-SBA-15(11)	433	42	0.644	0.015	54	n.d.[a]	n.d.
NiMo/Ti-SBA-15(19)	398	37	0.575	0.012	50	102	52
NiMo/Zr-SBA-15(17)	450	53	0.646	0.019	55	n.d.	n.d.
NiMo/Zr-SBA-15(22)	367	39	0.537	0.014	53	102	49

[a] Not determined.

Kubelka–Munk function, $F(R)^2$ versus energy (eV). The UV absorption edge, or optical band-gap (E_g, eV), was obtained by extrapolating to zero the linear region of the transformed DR UV–vis spectra. E_g values of 3.96 and 3.89 eV were determined for Ti-SBA-15 samples with 11 and 19 wt.% TiO_2, respectively. It is well known that E_g value strongly depends on the titania particle size. As compared with pure bulk anatase (E_g value of ca. 3.3 eV [41]), a blue shift of the band-gap absorption edge was observed for our Ti-SBA-15 samples. The magnitude of the detected blue shift diminishes as the titania loading increases. These data altogether allow to confirm that Ti is well dispersed in both Ti-SBA-15 samples. However, two kinds of Ti species coexist in each sample, isolated Ti species in tetrahedral coordination grafted on the SBA-15 surface by one or two Si–O–Ti linkages and some isolated or partially polymerized octahedral Ti species. At high TiO_2 loading, the increase in proportion of octahedral Ti species (probably small titania domains) is observed.

The UV–vis DRS spectra of Zr-SBA-15 samples are shown in Fig. 4B(d) and (e). The absorption band with maxima at about 200 nm is observed for both Zr-containing samples, regardless of zirconia loading. This band is attributable to LMCT transitions involving isolated Zr(IV) species in tetrahedral configuration [42,43]. Absorption at 230 nm, which is normally assigned to Zr(IV) species in other coordinations, was not observed. The absorption edge calculated for these samples (5.54 eV for Zr-SBA-15(17) and 5.52 eV for Zr-SBA-15(22) sample) is significantly larger than the E_g value previously reported for pure tetragonal zirconia (~5.2 eV) [42]. A shift of the absorption edge with increasing zirconia content was not as significant as in the case of Ti-modified samples indicating that zirconia species grafted on SBA-15 surface exist predominantly as isolated tetrahedrally coordinated Zr cations which are less susceptible to agglomeration than Ti species. Therefore, it can be concluded that only isolated extremely small zirconium oxide species are present on SBA-15 surface regardless of ZrO_2 loading.

From the results of characterizations described above, it is possible to conclude that chemical grafting allows preparation of Ti- or Zr-containing SBA-15 materials with relatively high TiO_2 or ZrO_2 loadings (19.2 and 22.4 wt.%, respectively) and without considerable damage of the initial SBA-15 structure. Titanium species are present on the SBA-15 surface predominantly as isolated tetrahedral species. However, at high TiO_2 loading an increase in the proportion of octahedral Ti species is observed. Zirconia species are present in isolated tetrahedral form at low and high ZrO_2 loading.

3.2. Catalysts in their oxidic state

The textural characteristics of NiMo catalysts supported on SBA-15 molecular sieves are given in Table 2. A significant decrease in BET surface area and total pore volume is observed when Ni and Mo are incorporated to the support. For all NiMo/SBA-15 catalysts the decrease in support surface area is much stronger (26–37%) that can be explained taking into account the weight of deposited Ni and Mo species. This decrease is more pronounced for the catalysts supported on pure siliceous SBA-15 and Ti-containing supports than for the catalysts supported on Zr-containing materials. A more detailed analysis of the changes in textural characteristics of samples after Ni and Mo

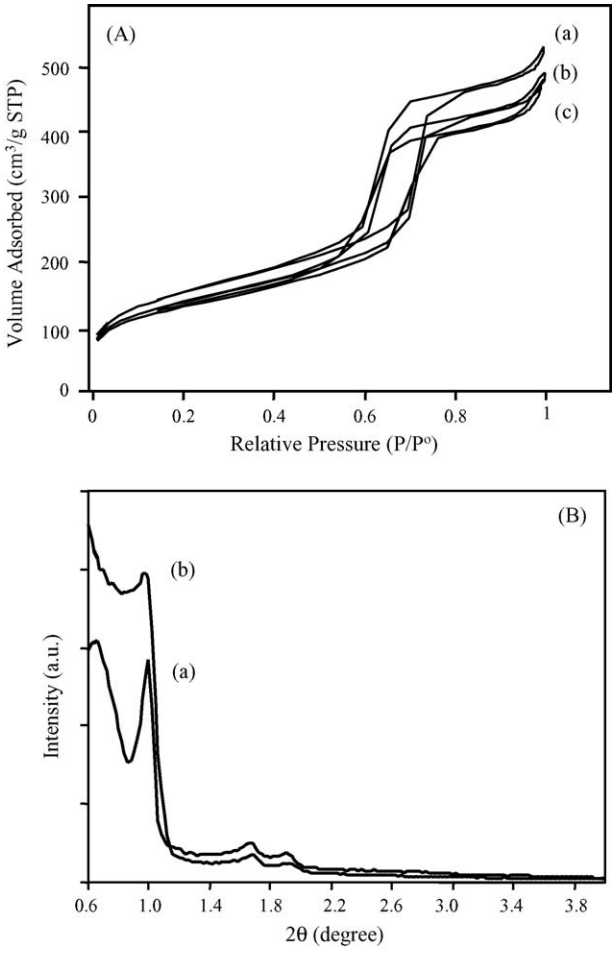

Fig. 5. N_2 adsorption–desorption isotherms (A) and small-angle XRD patterns (B) of NiMo/SBA-15 catalyst in oxidic (a) and sulfided (b and c) form: (b) before and (c) after catalytic test.

deposition reveals that micropore area decreases stronger (about 46–67%) than the mesopore area (21–32%). Similar tendency can also be observed for the changes in the micropore and mesopore volumes. Therefore, it can be concluded that some obstruction of the support pores or a partial collapse of its structure after metal deposition could take place in NiMo catalysts, being stronger the obstruction of micropores than of mesopores.

No changes were detected in the form of N_2 adsorption–desorption isotherms after successive incorporation of Mo and Ni species to the SBA-15 supports (Fig. 5A). A significant decrease in the amount of the adsorbed N_2 is observed after metal impregnation, especially after Mo deposition. However, the hysteresis loop maintains its shape characteristic of SBA-15 materials. In line with this, characteristic (1 0 0), (1 1 0) and (2 0 0) reflections of *p6mm* structure are still observed in the small-angle XRD pattern of all NiMo/SBA-15 catalysts (Fig. 5B). The intensity of these reflections becomes lower after Ni and Mo incorporation, probably due to the fact that Mo is a strong X-ray absorber [19] or because of a partial blocking of support channel system by oxidic metal species leading to some loss of long range order of mesostructure. Above results from nitrogen adsorption and XRD characterization show that the possibility of a partial collapse of SBA-15 structure after Ni and Mo deposition is low. Therefore, the obstruction of support pores, especially of the small ones (micropores), in NiMo catalysts seems to be more probable. It should be mentioned that the incorporation of Zr atoms in the SBA-15 support by post-synthetic chemical grafting slightly improves the catalyst textural characteristics (Table 2). Additionally, a small reduction of pore size (from 57 to 50–53 Å) is observed in NiMo catalysts supported on high loading Ti- and Zr-SBA-15 materials, which suggests that the deposited Mo and Ni oxide species are located inside the pores of Ti- or Zr-modified SBA-15 supports.

Powder XRD patterns for NiMo catalysts supported on different SBA-15 materials are shown in Fig. 6. As it was mentioned above, the XRD patterns of pure siliceous and Ti- or Zr-containing SBA-15 supports did not show the presence of any crystalline phase. In the case of NiMo catalysts supported on SBA-15 and Ti-SBA-15 supports, the diffraction lines corresponding to reflections of MoO_3 in orthorhombic phase (JCPDS card 35-609) were observed. The size of MoO_3 crystallites estimated using the Scherrer equation decreases from 723 Å (NiMo/SBA-15 catalyst) to 612 and 485 Å in NiMo/Ti-SBA-15(11) and NiMo/Ti-SBA-15(19) catalysts, respectively. The size of MoO_3 crystals compared to the pore diameter values of the used SBA-15 materials makes evident that they should be located on the external surface of the support particles. In contrast, for NiMo catalysts supported on Zr-modified SBA-15 materials, no XRD reflections were observed, showing a good dispersion of Ni and Mo oxidic species in these catalysts. This result can be attributed to the effect of zirconia incorporation in the SBA-15 supports on the dispersion of Ni and Mo oxidic species. Therefore, XRD characterization made evident that Ni and Mo oxidic species supported on Zr-containing materials and on pure siliceous or Ti-modified SBA-15 supports have different characteristics.

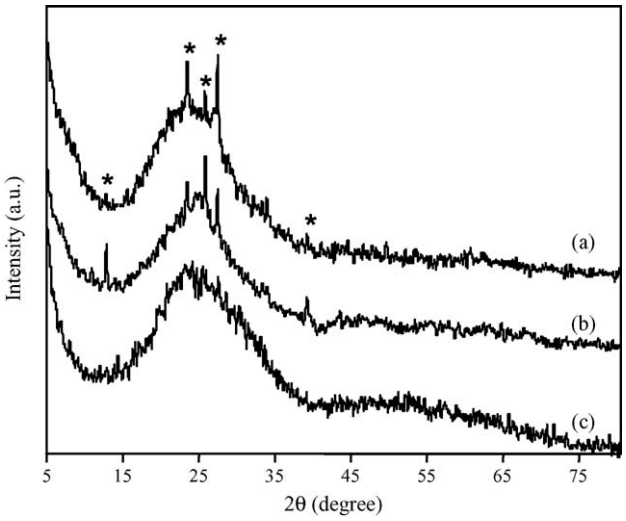

Fig. 6. Powder XRD patterns of NiMo catalysts supported on SBA-15 (a); Ti-SBA-15(19) (b); Zr-SBA-15(22) (c). (*) MoO_3, JCPDS card 35-609.

The TPR results for NiMo/SBA-15 catalysts are shown in Fig. 7. The TPR profile of the NiMo catalyst supported on pure siliceous SBA-15 sample exhibits two main reduction peaks at 450 and 700 °C and a shoulder at about 580–600 °C. The low temperature peak (450 °C) is generally associated to the reduction of Mo^{6+} to Mo^{4+} of polymeric octahedral Mo species weakly bound to the silica surface (probably small clusters of MoO_3) [44,45]. Comparing the present TPR pattern with TPR of bulk MoO_3 (main peak at 600 °C) [45], hydrogen consumption at 580–600 °C can be assigned to the reduction of crystalline MoO_3 phase detected by XRD. Finally, the peak at about 700 °C in the case of SiO_2-supported Mo catalysts is ascribed to the second step of reduction of the polymeric octahedral Mo species, from Mo^{4+} to Mo^0 [45,46]. The TPR characterization of NiMo catalyst supported on Ti-containing SBA-15 (Fig. 7b) shows that titanium grafting onto the SBA-15 surface leads to a slight increase in the temperature of Ni and Mo reduction because of their stronger interaction with the Ti-containing support. Thus, the first step of

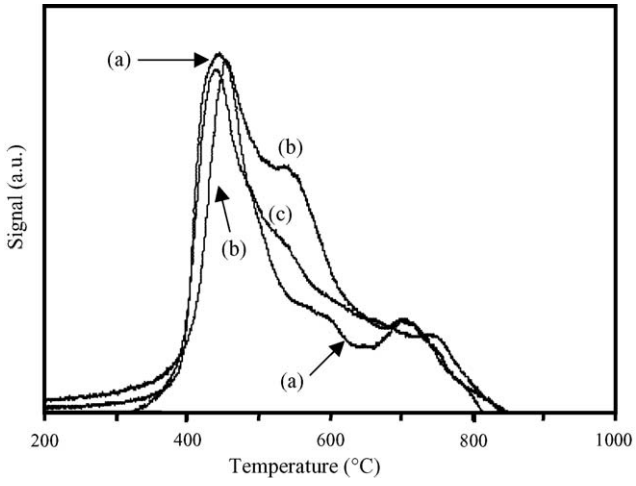

Fig. 7. TPR profiles for NiMo catalysts supported on SBA-15 (a); Ti-SBA-15(19) (b); Zr-SBA-15(22) (c).

reduction of octahedral Mo species in NiMo/Ti-SBA-15 samples takes place at 460 °C. Additionally, Ti incorporation in SBA-15 results in the shift of the second reduction peak ascribed to the reduction of polymeric MoO_3 species to lower temperature (560 °C) than in NiMo/SBA-15 sample. An increase in hydrogen consumption in this region is also observed indicating an increase in the proportion of polymeric octahedral Mo species after titania incorporation in the SBA-15 support. Similar effect induced by TiO_2 incorporation has been observed by us previously for SBA-16-supported catalysts and was attributed to the presence of Mo species interacting with titania particles [34]. The above changes in TPR profiles reflect the changes in the characteristics of Mo oxidic species in presence of titania, as it was evidenced by the decrease of MoO_3 crystal size (XRD results). On the contrary to the above results, Zr addition to the SBA-15 support leads to a decrease of the temperatures of different steps of reduction of Mo and Ni oxidic species (Fig. 7c), indicating easier reduction of octahedral molybdenum species supported on zirconia-containing support than those supported on SBA-15 and Ti-SBA-15. It appears that the reason for this is the better dispersion of Mo species on supports of Zr-SBA-15 series. In addition, it should be mentioned that in all TPR patterns presented in Fig. 7 reduction peaks in high temperature region (600–900 °C), with the exception of the peak at 700–750 °C, are not clearly defined showing the heterogeneity of Ni and Mo species in these catalysts. The first step of reduction of tetrahedral Mo species could also take place in this region. The presence of such species can be expected in some of our catalysts in view of previous reports, where the formation of tetrahedral or monomolybdate species were observed on zirconia or silica surface [5,11,47,48]. However, it is difficult to conclude about the presence of such species in our catalysts only on the basis of TPR results.

In order to obtain more information about the coordination and aggregation state of Ni and Mo oxidic species, UV–vis DRS spectra of NiMo catalysts were recorded (Fig. 8). Since Mo^{6+} has a d^0 electronic configuration, the only absorption due to LMCT transition, $O^{2-} \rightarrow Mo^{6+}$ is observed, which is expected in the range of 200–400 nm. As reported elsewhere [47,49,50], the absorption bands in 260–280 and 300–320 nm are assigned to the isolated molybdate (tetrahedral) and polymolybdate (octahedral) species, respectively. In addition, both types of Mo species show the second absorption band at about 230 nm. The DRS spectra of NiMo catalysts (Fig. 8A) show that in all the cases a mixture of Mo^{6+} ions species in tetrahedral (T_d) and octahedral (O_h) coordination is present. However, the proportion of different types of Mo species changes with the support composition. Thus, in the spectra of the catalysts supported on Ti-SBA-15 (Fig. 8) absorption band at about 300–330 nm becomes better defined and more intense than in the spectrum of the catalyst supported on pure siliceous SBA-15. At the same time, absorption in 260–280 nm region becomes less intense. It seems that titanium addition to the SBA-15 support leads to an increase in the proportion of O_h polymeric molybdenum species and to a decrease in the T_d ones. The absorption edges calculated for NiMo catalysts

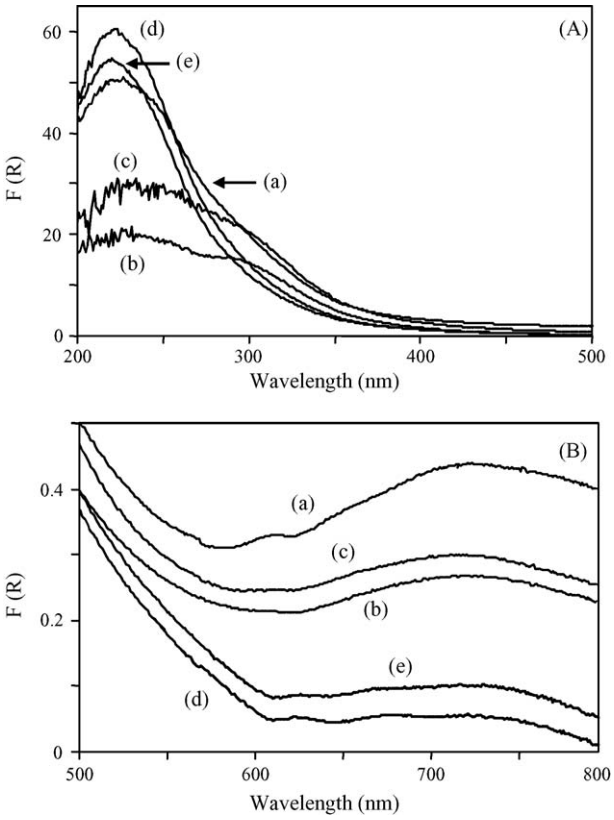

Fig. 8. UV–vis spectra of NiMo catalysts supported on SBA-15 (a); Ti-SBA-15(11) (b); Ti-SBA-15(19) (c); Zr-SBA-15(17) (d); Zr-SBA-15(22) (e). The spectrum of each support was subtracted from the spectrum of corresponding NiMo catalyst.

supported on SBA-15 and Ti-SBA-15 have values between 3.3 and 3.4 eV. These results are well in line with XRD observations where the presence of crystalline MoO_3 was detected for these catalysts. In contrast, in the spectra of Zr-SBA-15-supported NiMo catalysts absorption bands corresponding to the presence of O_h Mo species become less intense. As compared with spectra (a)–(c) in Fig. 8A, a blue shift of the band-gap absorption edge was observed for our NiMo/Zr-SBA-15 catalysts. E_g values calculated for these catalysts (3.9 eV for NiMo/Zr-SBA-15(17) and 4.1 eV for NiMo/Zr-SBA-15(22) catalyst) point out that a significantly better dispersion of Mo species takes place on the surface of Zr-modified SBA-15 materials. The magnitude of the detected blue shift increases with zirconia loading to the support. These data altogether allow confirming that tetrahedral or highly dispersed octahedral Mo species become dominating with zirconia loading to the SBA-15 support. The DRS spectra in the wavelength region corresponding to the absorption bands of Ni^{2+} ions are shown in Fig. 8B. Only the presence of octahedral Ni species in the form of NiO (bands at 720 nm) can be observed for all catalysts, regardless of the support used [47,51].

3.3. Sulfided catalysts

Sulfided NiMo catalysts were prepared by sulfidation at 400 °C for 4 h in a stream of 15 vol.% of H_2S in H_2 under

atmospheric pressure. In order to prove the extent of sulfidation of Mo species after the procedure, elemental analysis of sulfided NiMo/SBA-15 sample was performed. Supposing that only NiS and MoS_2 species are present in the sulfided catalyst, the degree of sulfidation was estimated as about 90–95%. Fig. 5A shows nitrogen adsorption–desorption isotherms of fresh sulfided NiMo/SBA-15 catalyst (curve b) and of the same catalyst after catalytic test (curve c). No changes were detected in the form of the isotherm after sulfidation of the catalyst and hydrodesulfurization of 4,6-DMDBT in comparison with the isotherm of oxidic precursor (curve a). A slight decrease in the amount of the adsorbed N_2 after sulfidation (Fig. 5A) may be due to the change in the density of the sulfided catalyst in comparison with its oxidic analog. However, the hysteresis loop maintains its shape characteristic of SBA-15 materials. In line with this, characteristic (1 0 0), (1 1 0) and (2 0 0) reflections of *p6mm* structure are still observed in the small-angle XRD pattern of the sulfided NiMo/SBA-15 catalyst (Fig. 5B, curve b). In fact, the intensity of (1 0 0) reflection is higher in the pattern of the sulfided catalyst than of the oxidic one. It seems that sulfidation of the catalyst results in some recovery of long range pore order of the support. Probably, large MoO_3 particles detected in the oxidic NiMo/SBA-15 catalyst by powder XRD disappear after sulfidation leading to MoS_2 particles of smaller size, and subsequently pore blockage produced by deposited Mo species diminishes. Above results from nitrogen adsorption and XRD characterization provide evidence for the conservation of the catalyst mesostructure after sulfidation and catalytic test.

In order to get more information about the dispersion of MoS_2 species, HRTEM and powder XRD characterizations of sulfided catalysts were performed. Fig. 9 shows the XRD pattern of fresh sulfided NiMo/SBA-15 catalyst (curve a). It can be observed that the reflections of crystalline MoO_3 detected in the diffractogram of the corresponding oxidic precursor (Fig. 6a) disappear after catalyst sulfidation. Instead of these reflections, new broad peaks corresponding to signals of hexagonal MoS_2 crystalline phase (JCPDS card 17-744) appear. Thus, the peak corresponding to *d*-spacing of MoS_2 phase ($d_{0\,0\,3}$ = 6.1 Å) can be observed at about 14.2° (2Θ). Wide peaks at about 33° and 58° (2Θ) correspond to ill-resolved reflections (1 0 1) and (1 1 0), respectively, of the same crystalline phase. The broadness of the reflections in Fig. 9 points out the small size of MoS_2 particles. Crystal size of MoS_2 roughly estimated from (0 0 2) reflection is about 43–45 Å, showing the decrease in particle size of Mo species in sulfided catalyst in comparison with the oxidic precursor where MoO_3 crystals with size of about 723 Å were found. The broad reflections of MoS_2 crystalline phase can still be observed in XRD pattern of the same sulfided catalyst after catalytic test (Fig. 9b). However, these signals disappear in the diffractogram of the sulfided NiMo catalyst supported on Zr-modified SBA-15, indicating better dispersion of MoS_2 phase in this catalyst.

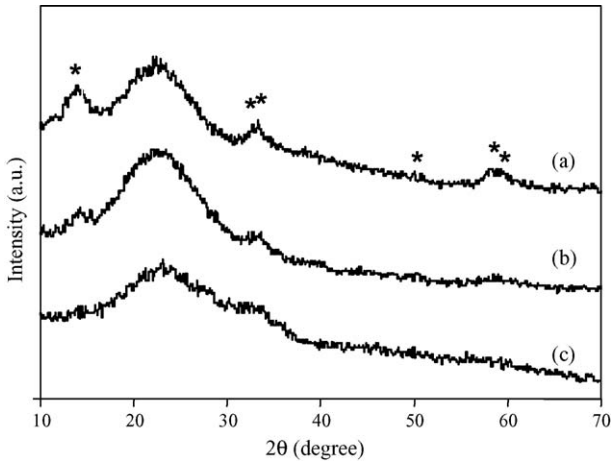

Fig. 9. Powder XRD patterns of sulfided NiMo/SBA-15 catalyst before (a) and after (b) catalytic test, and of fresh sulfided NiMo/Zr-SBA-15(22) catalyst (c). (*) MoS_2, JCPDS card 37-1492.

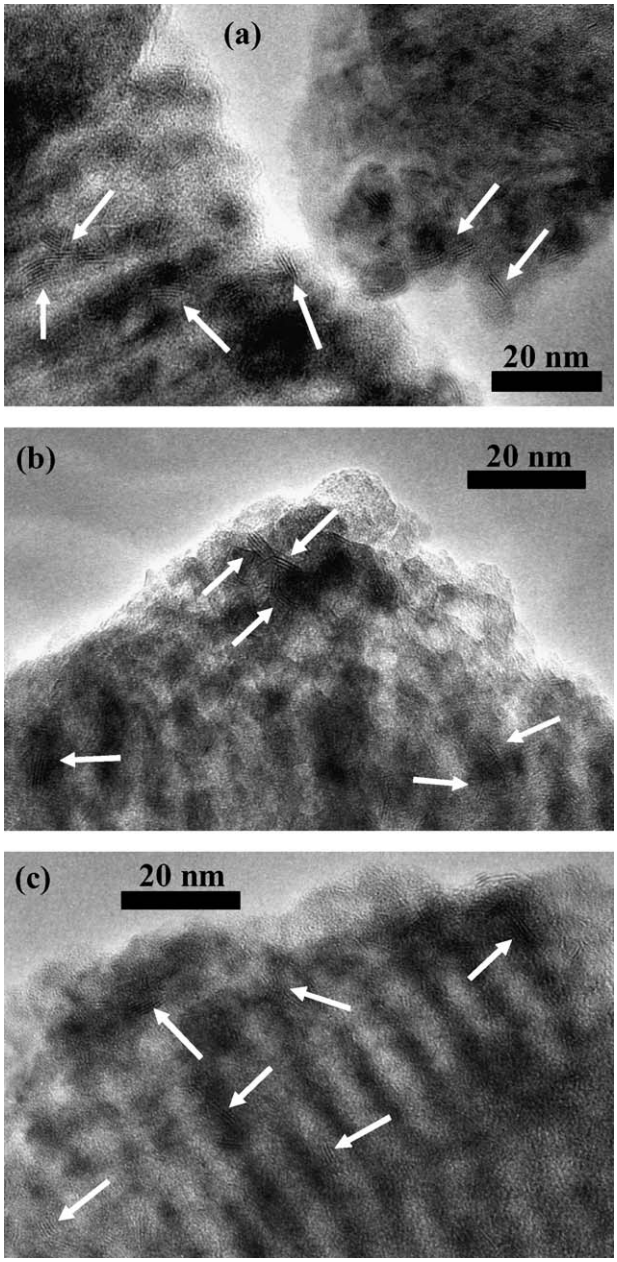

Fig. 10. HRTEM micrographs of sulfided NiMo catalysts supported on SBA-15 (a); Ti-SBA-15(19) (b); Zr-SBA-15(22) (c).

Table 3
Average length and layer number of the MoS_2 crystallites determined by HRTEM

Catalyst	Average length (Å)	Average stacking
NiMo/SBA-15	45	3.5
NiMo/Ti-SBA-15(19)	41	2.6
NiMo/Zr-SBA-15(22)	31	2.9

The suggested changes in the morphology of Mo species after Ti or Zr incorporation in the SBA-15 support were corroborated by HRTEM observations of the sulfided catalysts. The typical fringes due to MoS_2 crystallites with 6.2 Å interplanar distances were observed on micrographs of all sulfided catalysts (Fig. 10). Inhomogeneous dispersion of the MoS_2 phase can be seen in the catalyst supported on pure siliceous SBA-15 (Fig. 10a). MoS_2 crystallites with lengths between 20 and 60 Å and stacking from two to six layers are formed (Fig. 10a). In addition, some larger MoS_2 crystals (not shown) were also found on the external surface of SBA-15 particles. Titanium or zirconium incorporation in the support leads, as expected, to better dispersion of MoS_2 active phase (Fig. 10b and c). Average length and layer number of the MoS_2 crystallites are shown in Table 3. For all Ti- and Zr-containing supports, a decrease was observed in the stacking degree and length of MoS_2 particles. In addition, it should be mentioned that Ti incorporation resulted in a larger decrease in the stacking degree of the MoS_2 crystals than the Zr one. However, the MoS_2 structures are shorter on Zr-modified SBA-15 support than on Ti-SBA-15. In addition, a more detailed analysis of the slab length and stacking degree distributions in different NiMo/SBA-15 catalysts (Fig. 11) reveals that titanium and zirconium incorporation in the support results in more homogeneous distribution of MoS_2 particles in stacking degree and slab length.

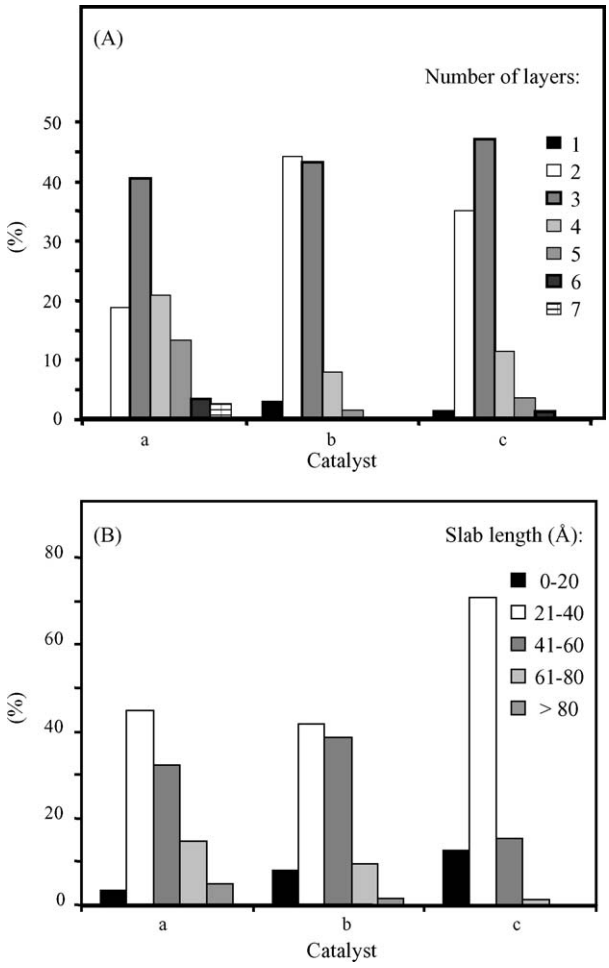

Fig. 11. Layer stacking (A) and length (B) distribution of MoS_2 crystallites in sulfided NiMo catalysts supported on SBA-15 (a); Ti-SBA-15(19) (b); Zr-SBA-15(22) (c).

3.4. Catalytic activity

In the present study, the catalytic activity of sulfided NiMo/SBA-15 catalysts was examined in the hydrodesulfurization of 4,6-dimethyldibenzothiophene, one of the most refractory sulfur compounds in gas oil [52]. The conversion of 4,6-DMDBT is shown in Table 4. It can be observed that 4,6-DMDBT conversion reached at 8 h changes in a wide range. Thus, the lowest 4,6-DMDBT conversion (56%) was observed for the catalyst supported on purely siliceous SBA-15. Catalytic activities of all NiMo catalysts supported on Ti- or Zr-modified SBA-15 resulted to be significantly higher than that of the reference NiMo/SBA-15 catalyst and previously reported NiMo catalyst supported on SBA-16 modified with 15 wt.%

Table 4
4,6-DMDBT conversions and HYD/DDS pathway ratios obtained over NiMo/SBA-15 catalysts

Catalyst	4,6-DMDBT conversion (%)[a]								HYD/DDS ratio[b]
	1	2	3	4	5	6	7	8	
NiMo/SBA-15	8	14	23	30	36	43	50	56	7.4
NiMo/Ti-SBA-15(11)	9	20	31	40	49	59	67	74	8.1
NiMo/Ti-SBA-15(19)	13	26	38	50	63	75	82	88	9.8
NiMo/Zr-SBA-15(17)	11	21	33	46	57	69	77	84	9.7
NiMo/Zr-SBA-15(22)	15	29	44	60	72	82	87	92	10.0
Reference NiMo/γ-Al_2O_3	7	15	25	33	42	51	57	61	11.4

[a] At different reaction time (h).
[b] Determined at 30% of total 4,6-DMDBT conversion. DDS, direct desulfurization pathway; HYD, hydrogenation pathway; THDMDBT, tetrahydrodimethyldibenzothiophene; HHDMDBT, hexahydrodimethyldibenzothiophene; MCHT, methylcyclohexyltoluene; DMBP, dimethylbiphenyl; DMBCH, dimethylbicyclohexyl. HYD/DDS pathway ratio was determined as the ratio of HYD route products (THDMDBT + HHDMDBT + MCHT + DMBCH) to DDS route product (DMBP) [52].

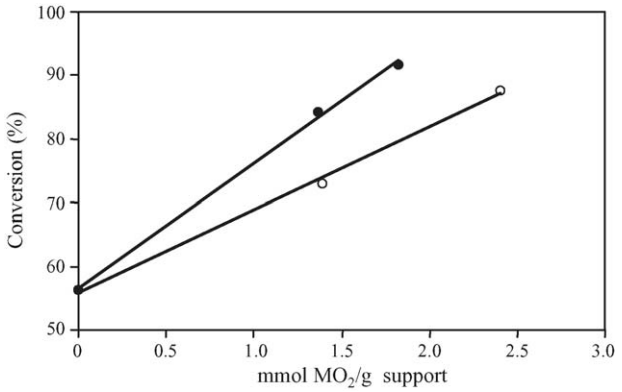

Fig. 12. Correlation between 4,6-DMDBT conversion at 8 h reaction time and titania or zirconia loading in the catalytic support. $MO_2 = TiO_2$ (○) or ZrO_2 (●).

of TiO_2 by similar grafting procedure which gave 65% of 4,6-DMDBT conversion at 8 h [34]. Moreover, catalytic activity increased with increasing TiO_2 or ZrO_2 loading in the support. The maximum conversion of 92% was reached with NiMo/Zr-SBA-15(22) catalyst. Almost linear correlation can be observed between 4,6-DMDBT conversion reached at 8 h reaction time and titania or zirconia loading in the support (Fig. 12). In addition, Fig. 12 shows that zirconia containing NiMo/SBA-15 catalysts showed higher catalytic activity that the Ti-containing ones with similar MO_2 loading. This result is in accordance with previous report [7], where catalytic activities of NiMo catalysts supported on pure TiO_2 and ZrO_2 were compared in thiophene hydrodesulfurization. NiMo catalysts supported on zirconia were found to be more active than the titania supported counterparts. In our case, the activity trend with the change in the TiO_2 or ZrO_2 content in the SBA-15 support seems to be the result of the changes in the dispersion of oxidic and sulfided Mo active species. Thus, the incorporation of titanium onto the support surface provides a stronger metal–support interaction, allowing better dispersion of the molybdenum and nickel phases. In addition, an increase in the proportion of octahedrally coordinated Mo species was found in NiMo/Ti-SBA-15 catalysts in comparison to that supported on pure siliceous SBA-15. This explains an increase in 4,6-DMDBT conversion with TiO_2 loading in NiMo/Ti-SBA-15 catalysts. On the other hand, when zirconia is incorporated on the SBA-15 surface, characteristics of Mo active species change stronger than after Ti incorporation. In Zr-SBA-15-supported catalysts, Mo oxidic species are present in tetrahedral or highly dispersed octahedral form and they are easy to reduce. High dispersion of Mo is still observed in sulfided NiMo/Zr-SBA-15 catalysts. Therefore, an increase in the total amount of HDS active sites can be expected in NiMo/Zr-SBA-15 catalysts in comparison to SBA-15- and Ti-SBA-15-supported ones.

In order to compare the activity of our NiMo/SBA-15 catalysts and of the reference NiMo/γ-Al_2O_3 catalyst, initial reaction rates of 4,6-DMDBT HDS and corresponding pseudo-first-order rate constants were calculated (Table 5). It can be observed from Table 5 that the catalytic activity of SBA-15-supported catalysts increases in the following order: NiMo/SBA-15 < NiMo/γ-Al_2O_3 < NiMo/Ti-SBA-15(11) < NiMo/Zr-SBA-15(17) < NiMo/Ti-SBA-15(19) < NiMo/Zr-SBA-15(22). Pseudo-first-order rate constants determined for different NiMo/SBA-15 catalysts changes between 4.44×10^{-6} and 1.11×10^{-5} L/(s g catalyst) (Table 5). For the reference NiMo/γ-Al_2O_3 catalyst tested in 4,6-DMDBT HDS under similar reaction conditions, the rate constant value of 5.18×10^{-6} L/(s g catalyst) was calculated. Therefore, it can be concluded that all our catalysts supported on Ti- or Zr-doped SBA-15 are significantly more active than the alumina-supported analog in HDS of refractory dibenzothiophenes, such as 4,6-DMDBT. The best catalyst, NiMo/Zr-SBA-15(22), is twice more active than NiMo/γ-Al_2O_3.

Table 5
Initial reaction rates and pseudo-first-order rate constants obtained for 4,6-DMDBT HDS over NiMo/SBA-15 catalysts[a]

Catalyst	Initial reaction rate (mol/(L s g catalyst))	Pseudo-first-order rate constant (L/(s g catalyst))
NiMo/SBA-15	2.66×10^{-6}	4.44×10^{-6}
NiMo/Ti-SBA-15(11)	4.00×10^{-6}	6.67×10^{-6}
NiMo/Ti-SBA-15(19)	5.78×10^{-6}	9.63×10^{-6}
NiMo/Zr-SBA-15(17)	4.89×10^{-6}	8.15×10^{-6}
NiMo/Zr-SBA-15(22)	6.67×10^{-6}	1.11×10^{-5}
Reference NiMo/γ-Al_2O_3	3.11×10^{-6}	5.18×10^{-6}

[a] Reaction conditions: batch reactor using 40 mL of 4,6-DMDBT solution in *n*-hexadecane (0.024 mol/L), 0.15 g of catalyst, 300 °C, 7.3 MPa.

Nowadays, it is known that the HDS of methyl-substituted DBT derivatives occurs through two parallel reactions, namely, (i) direct desulfurization (DDS) yielding the corresponding substituted biphenyl (BP) products and (ii) hydrogenation with subsequent desulfurization (HYD), yielding first substituted tetrahydrodibenzothiophenes, then the corresponding hexahydro-derivatives and, finally, cyclohexylbenzene-type compounds [53,54]. Previously, it has been shown that under HDS conditions (*i.e.*, in presence of an organic sulfur compound) biphenyl-type compounds do not hydrogenate readily into cyclohexylbenzene [55]. To elucidate the effect of Ti and Zr incorporation in the supports on the reaction pathways of 4,6-dimethyldibenzothiophene, the reaction product distributions at the same total 4,6-DMDBT conversion (30%) was compared for different catalysts (Table 4). The HYD/DDS ratios from Table 4 show that for all catalysts studied the preferential pathway is HYD. When Ti- or Zr-atoms are incorporated into the SBA-15 support, the proportion of HYD route products increases, reaching the maximum HYD/DDS ratio of 10.0 for the most active catalyst, NiMo/Zr-SBA-15(22). Therefore, our results allow to conclude that Ti or Zr incorporation in SBA-15 support leads to an increase in hydrogenation activity of the catalyst, and by this means HYD route of hydrodesulfurization of 4,6-DMDBT is promoted. NiMo catalysts supported on Zr-SBA-15 show higher HYD/DDS ratio than the catalysts supported on Ti-SBA-15. This should be related with the morphology of MoS_2 active phase observed by HRTEM. It seems that MoS_2 crystals on Zr-SBA-15 surface, formed by ~3 short slabs, have the best ratio

length/slabs number for 4,6-DMDBT elimination. Previously it has already been reported [27] that zirconium addition into NiMo catalysts supported on HMS improves their hydrogenation activity. However, when NiMo/Zr-HMS catalysts were evaluated in thiophene HDS, a linear decrease of thiophene conversion was observed with an increase of zirconium content. This result differs from our observations for the case of 4,6-DMDBT, where both hydrogenation ability (HYD/DDS ratio) and total activity increase simultaneously. This difference may be due, probably, to the fact that HDS of refractory sulfur compounds, such as 4,6-DMDBT, occurs preferentially through HYD pathway, whereas the desulfurization of more reactive sulfur compounds normally takes place via DDS pathway.

4. Conclusions

According to the above results, the following conclusions can be stated.

Ti- and Zr-containing SBA-15 type materials with relatively high TiO_2 or ZrO_2 loadings (19.2 and 22.4 wt.%, respectively) and without considerable degradation of the initial SBA-15 pore structure can be prepared by chemical grafting method. Chemical grafting resulted to be a suitable experimental technique leading to Ti-SBA-15 and Zr-SBA-15 supports with highly dispersed metal (Ti, Zr) species. Isolated tetrahedral Ti and Zr species are present predominantly on the SBA-15 surface. However, at high TiO_2 loading an increase in the proportion of octahedral Ti species is observed.

The interaction of Ni and Mo species with the SBA-15 support becomes stronger with TiO_2 or ZrO_2 loading. According to this, the dispersion of oxidic and sulfided Mo species increases, especially for Zr-containing SBA-15 supports.

NiMo catalysts supported on Ti- and Zr-containing SBA-15 molecular sieves show high activity in HDS of refractory dibenzothiophenes (4,6-DMDBT). The activity increases almost linearly with titania or zirconia loading in the support reaching the maximum catalytic activity at 22.4 wt.% of ZrO_2 loading. High catalytic activity shown by NiMo/Ti-SBA-15 and NiMo/Zr-SBA-15 catalysts seems to be related with their high hydrogenation activity and promotion of HYD pathway of 4,6-DMDBT HDS. The changes observed in catalytic activity and selectivity of NiMo/SBA-15 catalysts studied are due to the changes in the morphology of MoS_2 active phase (length and number of slabs) induced by incorporation of Ti or Zr atoms in the support.

Finally it can be concluded that high-performance catalysts for HDS of refractory dibenzothiophenes can be prepared using SBA-15 supports modified with titania and zirconia.

Acknowledgements

Financial support by CONACYT-Mexico (grant 46354-Y) is gratefully acknowledged. The authors wish to thank M. Aguilar Franco and I. Puente Lee for technical assistance with small-angle XRD and HRTEM characterizations, respectively.

References

[1] B.C. Gates, H. Topsøe, Polyhedron 16 (1997) 3213.
[2] F. van Looij, P. van der Laan, W.H.J. Stork, D.J. DiCamillo, J. Swain, Appl. Catal. A: Gen. 170 (1998) 1.
[3] H. Shimada, T. Sato, Y. Yoshimura, J. Hiraishi, A. Nishijima, J. Catal. 110 (1988) 275.
[4] Y.I. Yermakov, A.N. Startsev, V.A. Burmistrov, Appl. Catal. 11 (1984) 1.
[5] M. Jia, P. Afanasiev, M. Vrinat, Appl. Catal. A: Gen. 278 (2005) 213.
[6] S.K. Maity, M.S. Rana, B.N. Srinivas, S.K. Bej, G. Murali Dhar, T.S.R. Prasad Rao, J. Mol. Catal. A 153 (2000) 127.
[7] M. Jia, P. Afanasiev, M. Vrinat, W. Li, H. Xu, Q. Ge, Petrochem. Technol. 33 (2004) 202.
[8] H. Shimada, Catal. Today 86 (2003) 17.
[9] J.J. Lee, S. Han, H. Kim, J.H. Koh, T. Hyeon, S.H. Moon, Catal. Today 86 (2003) 141.
[10] J.G. Weissman, E.C. DeCanio, J.C. Edwards, Catal. Lett. 24 (1994) 113.
[11] J. Ramírez, R. Cuevas, P. Castillo, M.L. Rojas, T. Klimova, Bulg. Chem. Commun. 30 (1998) 207.
[12] S. Damyanova, L. Petrov, P. Grange, Appl. Catal. A: Gen. 239 (2003) 241.
[13] M.S. Rana, S.K. Maity, J. Ancheyta, G. Murali Dhar, T.S.R. Prasada Rao, Appl. Catal. A: Gen. 268 (2004) 89.
[14] M.C. Barrera, M. Viniegra, J. Escobar, M. Vrinat, J.A. de los Reyes, F. Murrieta, J. García, Catal. Today 98 (2004) 131.
[15] A. Wang, Y. Wang, T. Kabe, Y. Chen, A. Ishihara, W. Qian, J. Catal. 199 (2001) 19.
[16] T. Klimova, M. Calderón, J. Ramírez, Appl. Catal. A: Gen. 240 (2003) 29.
[17] U.T. Turaga, C. Song, Catal. Today 86 (2003) 129.
[18] A. Wang, Y. Wang, T. Kabe, Y. Chen, A. Ishihara, W. Qian, P. Yao, J. Catal. 210 (2002) 319.
[19] A. Sampieri, S. Pronier, J. Blanchard, M. Breysse, S. Brunet, K. Fajerwerg, C. Louis, G. Pérot, Catal. Today 107/108 (2005) 537.
[20] L. Vradman, M.V. Landau, M. Herskowitz, V. Ezersky, M. Talianker, S. Nikitenko, Y. Koltypin, A. Gedanken, J. Catal. 213 (2003) 163.
[21] G. Murali Dhar, B.N. Srinivas, M.S. Rana, M. Kumar, S.K. Maity, Catal. Today 86 (2003) 45.
[22] M. Breysse, P. Afanasiev, C. Geantet, M. Vrinat, Catal. Today 86 (2003) 5.
[23] S. Yoshinaka, K. Segawa, Catal. Today 45 (1998) 293.
[24] Z.B. Wei, W. Yan, H. Zhang, T. Ren, Q. Xin, Z. Li, Appl. Catal. A: Gen. 167 (1998) 39.
[25] S. Dzwigaj, C. Louis, M. Breysse, M. Cattenot, V. Bellière, C. Geantet, M. Vrinat, P. Blanchard, E. Payen, S. Inoue, H. Kudo, Y. Yoshimura, Appl. Catal. B: Environ. 41 (2003) 181.
[26] T. Klimova, E. Rodríguez, M. Martínez, J. Ramírez, Micropor. Mesopor. Mater. 44/45 (2001) 357.
[27] N.G. Kostova, A.A. Spojakina, K. Jiratova, O. Solcova, L.D. Dimitrov, L.A. Petrov, Catal. Today 65 (2001) 217.
[28] P.J. Kooyman, P. Waller, A.D. van Langeveld, C. Song, K.M. Reddy, J.A.R. van Veen, Catal. Lett. 90 (2003) 131.
[29] Z. Li, L. Gao, S. Zheng, Appl. Catal. A: Gen. 236 (2002) 163.
[30] D. Zhao, J. Feng, Q. Huo, N. Melosh, G.H. Fredrickson, B.F. Chmelka, G.D. Stucky, Science 279 (1998) 548.
[31] D. Zhao, Q. Huo, J. Feng, B.F. Chmelka, G.D. Stucky, J. Am. Chem. Soc. 120 (1998) 6024.
[32] T. Yamada, H. Zhou, K. Asai, I. Honma, Mater. Lett. 56 (2002) 93.
[33] T. Klimova, L. Lizama, J.C. Amezcua, P. Roquero, E. Terrés, J. Navarrete, J.M. Domínguez, Catal. Today 98 (2004) 141.
[34] J.C. Amezcua, L. Lizama, C. Salcedo, I. Puente, J.M. Domínguez, T. Klimova, Catal Today 107–108 (2005) 578.
[35] M. Impéror-Clerc, P. Davidson, A. Davidson, J. Am. Chem. Soc. 122 (2000) 11925–11933.
[36] Z. Luan, E.M. Maes, P.A.W. van der Heide, D. Zhao, R.S. Czernuszewicz, L. Kevan, Chem. Mater. 11 (1999) 3680.
[37] I.G. Shenderovich, G. Buntkowsky, A. Schreiber, E. Gedat, S. Sharif, J. Albrecht, N.S. Golubev, G.H. Findenegg, H.-H. Limbach, J. Phys. Chem. B 107 (2003) 11924.

[38] S. Srinivasan, A.K. Datye, M.H. Smith, C.H.F. Peden, J. Catal. 145 (1994) 565.
[39] S. Klien, B.M. Weckhuysen, J.A. Martens, W.F. Maier, P.A. Jacobs, J. Catal. 163 (1996) 489.
[40] G. Petrini, A. Cesana, G. De Alberti, F. Genoni, G. Leofanti, M. Padovan, G. Paparatto, P. Roffia, Stud. Surf. Sci. Catal. 68 (1991) 761.
[41] X. Gao, I.E. Wachs, Catal. Today 51 (1999) 233.
[42] X. Gao, J.L.G. Fierro, I.E. Wachs, Langmuir 15 (1999) 3169.
[43] B. Rakshe, V. Ramaswamy, S.G. Hegde, R. Vetrivel, A.V. Ramaswamy, Catal. Lett. 45 (1997) 41.
[44] R. López Cordero, A. López Agudo, Appl. Catal. A: Gen. 202 (2000) 23.
[45] R. López Cordero, F.J. Gil Llambias, A. López Agudo, Appl. Catal. 74 (1991) 125.
[46] S. Damyanova, A. Spojakina, K. Jiratova, Appl. Catal. A: Gen. 125 (1995) 257.
[47] Z. Liu, Y. Chen, J. Catal. 177 (1998) 314.
[48] C. Louis, M. Che, M. Anpo, J. Catal. 141 (1993) 453.
[49] C.C. Williams, J.G. Ekerdt, J.-M. Jehng, F.D. Hardcastle, A.M. Turek, I.E. Wachs, J. Phys. Chem. 95 (1991) 8781.
[50] C.C. Williams, J.G. Ekerdt, J.-M. Jehng, F.D. Hardcastle, I.E. Wachs, J. Phys. Chem. 95 (1991) 8791.
[51] B. Scheffer, J.J. Heijeinga, J.A. Moulijn, J. Phys. Chem. 91 (1987) 4752.
[52] B.C. Gates, H. Topsøe, Polyhedron 16 (1997) 3213.
[53] C. Pophal, F. Kameda, K. Hoshino, S. Yoshinaka, K. Segawa, Catal. Today 39 (1997) 21.
[54] F. Bataille, J.L. Lemberton, P. Michaud, G. Pérot, M. Vrinat, M. Lemaire, E. Schulz, M. Breysse, S. Kasztelan, J. Catal. 191 (2000) 409.
[55] P. Michaud, J.L. Lemberton, G. Pérot, Appl. Catal. A: Gen. 169 (1998) 343.